ACS Catalysis

Research Article

pubs.acs.org/acscatalysis

Design of Lewis Pair-Functionalized Metal Organic Frameworks for CO_2 Hydrogenation

Jingyun Ye[†] and J. Karl Johnson*[,†,‡]

[†]Department of Chemical & Petroleum Engineering, University of Pittsburgh, Pittsburgh, Pennsylvania 15261, United States

[‡]National Energy Technology Laboratory, Pittsburgh, Pennsylvania 15236, United States

Supporting Information

ABSTRACT: Efficient catalytic reduction of CO_2 is critical for the large-scale utilization of this greenhouse gas. We have used density functional electronic structure methods to design a catalyst for producing formic acid from CO_2 and H_2 via a two-step pathway having low reaction barriers. The catalyst consists of a microporous metal organic framework that is functionalized with Lewis pair moieties. These functional groups are capable of chemically binding CO_2 and heterolytically dissociating H_2. Our calculations indicate that the porous framework remains stable after functionalization and chemisorption of CO_2 and H_2. We have identified a low barrier pathway for simultaneous addition of hydridic and protic hydrogens to carbon and oxygen of CO_2, respectively, producing a physisorbed HCOOH product in the pore. We find that activating H_2 by dissociative adsorption leads to a much lower energy pathway for hydrogenating CO_2 than reacting H_2 with chemisorbed CO_2. Our calculations provide design strategies for efficient catalysts for CO_2 reduction.

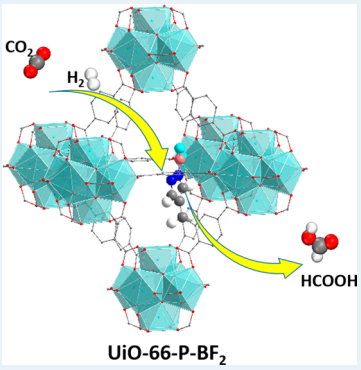

KEYWORDS: *catalytic reduction of CO_2, UiO-66, Lewis acids, Lewis bases, density functional theory, metal-free catalysis*

INTRODUCTION

Efficient conversion of CO_2 from various emission sources into valuable chemicals has the potential to reduce net CO_2 emissions while generating high-energy density fuels and other commodities.[1−6] However, reduction of CO_2 is very challenging because of its chemical inertness and thermodynamic stability, which typically requires aggressive reaction conditions (high temperature and high pressure). It has been assumed that reduction of CO_2 under mild conditions requires the activation of CO_2, usually with an organometallic catalyst.[7] Indeed, catalytic hydrogenation of CO_2 to formic acid (HCOOH) is most commonly accomplished via homogeneous catalysis with organometallic complexes containing rhodium, ruthenium, or iridium.[8,9] Heterogeneous hydrogenation of CO_2 can be accomplished on metal surfaces such as Ni[10−13] and Cu,[14,15] but these reactions have higher barriers than homogeneous catalysts and, hence, require higher temperatures.[8]

Perhaps the most simple and direct route for CO_2 reduction is the addition of a proton (to the oxygen atom) and a hydride (to the carbon atom) to produce HCOOH. Conceptually, the required protic and hydridic hydrogens can be provided by Lewis bases and acids, respectively. Indeed, it has been experimentally shown that frustrated Lewis pairs (FLPs) can both bind CO_2 and heterolytically dissociate H_2.[16,17] As a result, FLPs have been considered as excellent candidates for both CO_2 activation and subsequent stepwise hydrogenation for the production of hydrogen-rich C1 fuels.[18−21]

FLPs require significant steric hindrance to prevent the formation of Lewis acid/Lewis base adducts in solution, which would render them completely inactive. These very bulky substituents, however, may increase the energy required to activate the reactants.[18] It is therefore important to explore other possibilities to stabilize Lewis pairs (LPs) that do not involve steric hindrance. In this work, we propose incorporating LPs into nanoporous materials such as metal organic frameworks (MOFs) as a platform for catalytically reducing CO_2 with H_2.

Our hypothesis is that LP-functionalized MOFs will retain the chemical activity of FLPs for binding CO_2 and dissociating H_2. These LP-MOFs should be active for the reduction of CO_2 to formic acid. The geometric constraint of the LPs' being covalently bound to the MOF at specific sites will prevent mutual quenching of a pair of LP moieties within the pore, without the need for steric hindrance.

Although homogeneous catalysts have lower reaction barriers for CO_2 hydrogenation compared with extant heterogeneous catalysts, they also have significant drawbacks. Our proposed LP-functionalized MOF catalyst combines the advantages of each and thereby bridges the gap between homo- and heterogeneous catalysis.[22,23] The potential advantages of our proposed catalyst include (1) metal-free catalytic sites, reducing the cost of the catalyst; (2) ease of catalyst separation/recycle and product recovery;[6] (3) the potential to combine the CO_2 capture and conversion steps in a single material;[24−26] (4) improved mass transfer performance compared with liquid

Received: February 23, 2015
Revised: March 23, 2015
Published: April 1, 2015

DOI: 10.1021/acscatal.5b00396
ACS Catal. 2015, 5, 2921−2928

phase reactions, in which gas−liquid mass transfer resistance and solubilities are often limiting; (5) good thermal stability, allowing for a wide range of operating temperatures; (6) pore environments that can potentially be tuned to increase the reactivity (e.g., through confinement and orientational restrictions); and (7) low reaction barriers, allowing CO_2 reduction under mild conditions.

We have chosen UiO-66 (Figure S1) as a candidate MOF for LP functionalization because it is chemically and thermally stable,[27−32] highly selective toward CO_2 adsorption,[29,33−36] and can be readily functionalized via various approaches.[27,28,30,33−35,37−41] In this work, we carry out density functional theory calculations using the CP2K code,[42] including dispersion corrections,[43] to test our hypothesis that LP-functionalized MOFs can be used to catalyze the reduction of CO_2 to formic acid with H_2.

It is important at the outset to establish whether UiO-66 or similar MOFs can be expected to be functionalized with moieties of the size and complexity of LP functional groups. There are three possible routes to functionalize MOFs, including robust Zr-based materials such as UiO-66 and its analogous. These include mixed ligand synthesis,[30,33,38,41,44−46] postsynthetic modification (PSM),[28,30,39,47−49] and postsynthetic ligand exchange (PSE).[30,38,46] We note that all three methods have been used to functionalize Zr-based MOFs with large complex functional groups. For example, Wang et al. functionalized UiO-67 with a series of photocatalysts, demonstrating activity for H_2O oxidation and CO_2 reduction.[44,45] Garibay et al. have used PSM to functionalize UiO-66 with a variety of anhydrides, including octanoic and maleic anhydride,[28] which are larger than the LP group we investigate in this work. The PSE method has been used to introduce a bulky photocatalyst into UiO-66.[38] These examples demonstrate that catalytic moieties can be covalently bonded into UiO-based MOFs and that the resulting functionalized MOFs are very stable and can have enhanced catalytic activity due to stabilization or protection of the catalytic complexes. It is therefore reasonable to expect that functional groups containing LP moieties can be incorporated into UiO-66 or related MOFs, although, to the best of our knowledge, this has not yet been attempted.

METHODS

Periodic DFT calculations were carried out in the mixed Gaussian plane wave scheme as implemented in the CP2K[42] code with Grimme's D3 dispersion corrections.[43] The PBE functional[50] was used to calculate the exchange correlation energy. The DZVP-MOLOPT basis set in combination with Geodecker, Teter, and Hutter pseudopotentials[51] were used with a plane wave cutoff energy of 360 Ry. The adequacy of the basis set and energy cutoff parameters have been confirmed by multiple test calculations (see Table S1 and Figure S2 in the Supporting Information). We have also checked the accuracy of the PBE functional by comparing calculations on related molecular species using the CP2K and Gaussian 09[52] codes. We found that the PBE functional gives adsorption energies that are in good agreement (average absolute deviation of 0.05 eV) with second-order Møller−Plesset perturbation theory, coupled cluster with single, double, and perturbational triple excitation calculations, and calculations with the M06-2X functional (see Tables S2 and S3 in the Supporting Information).

The unit cell of UiO-66 (Figure S1a) was taken from the Cambridge Crystallographic Data Centre (CCDC deposition number: 8895295[35]), and calculations were carried out on the primitive cell (Figure S1b) to save computational effort. The lattice constants of the optimized primitive cell are $a = b = c =$ 14.788 Å, $\alpha = \beta = \gamma = 60°$ and correspond to the unit cell with $a = b = c =$ 20.913 Å, $\alpha = \beta = \gamma = 90°$. These values are in very good agreement with published experimental[27,32,53] and computational[31,32,35] data.

We selected the FLP 1-[bis(pentafluorophenyl)boryl]-3,5-di*tert*-butyl-1H-pyrazole[54,55] (**FLP1**, Figure 1a) as the parent

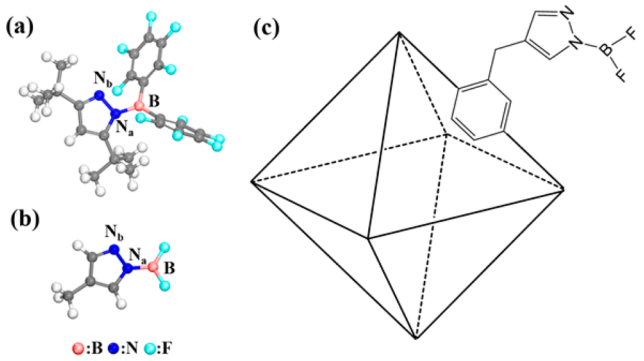

Figure 1. (a) Structure of 1-[bis(pentafluorophenyl)boryl]-3,5-di-*tert*-butyl-1*H*-pyrazole, **FLP1**. (b) Structure of 1-(difluoroboranyl)-4-methyl-1*H*-pyrazole, denoted as P-BF_2. (c) Schematic of a UiO-66 primitive cell functionalized with P-BF_2.

structure for our candidate LP functional groups because it has both Lewis acid (B) and base (N_b) sites within a single molecule and shows the ability to heterolytically cleave H_2 and bind CO_2.[54,55] We have modified **FLP1** by removing the *tert*-butyl groups and replacing the bulky C_6F_5 moieties with F atoms. We have also added a methyl group to link with the 1,4-benzenedicarboxylate (BDC) linkers of the MOF framework. The resulting molecule (1-(difluoroboranyl)-4-methyl-1*H*-pyrazole), which we name P-BF_2, is shown in Figure 1b. P-BF_2 is a Lewis pair without steric hindrance, which would form a dimer in solution, quenching the Lewis acid (B) and base (N_b) sites. However, binding P-BF_2 to BDC linkers of UiO-66 prevents migration and association of P-BF_2 groups (Figure 1c).

In this work, we examine the case of one P-BF_2 group per UiO-66 primitive cell (four per unit cell) and denote this system as UiO-66-P-BF_2. Future work will explore multiple functional groups per primitive cell. We found that fully relaxing the geometry and cell parameters of UiO-66-P-BF_2 gave lattice constants that were almost identical to the relaxed UiO-66 values. Furthermore, optimizing the structure with chemisorbed CO_2 or H_2 in UiO-66-P-BF_2 also perturbed the lattice constants and energies by a very minor amount (see Table S4 in the Supporting Information). Therefore, we held the lattice constants fixed at the ground state UiO-66 values for most calculations to save computational time.

The adsorption energies of H_2 or CO_2 were defined as

$$E_{ad}(M) = E(M/\text{UiO-66-P-BF}_2) - E(\text{UiO-66-P-BF}_2) - E(M) \quad (1)$$

where M represents either H_2 or CO_2 and E(M/UiO-66-P-BF_2), E(UiO-66-P-BF_2), and E(M) represent the total energies of the UiO-66-P-BF_2 with the adsorbate, the empty UiO-66-P-BF_2, and the gas phase adsorbate, respectively. In the case of

DOI: 10.1021/acscatal.5b00396
ACS Catal. 2015, 5, 2921−2928

coadsorption, the relative energies were computed with respect to the sum of the total energies of the corresponding gas phase molecules. Zero-point energy (ZPE) corrections were applied to all the energy values. Comparison of the energies with and without ZPE corrections are provided in the Supporting Information (Figures S13–S15). Equation 1 defines negative values as exothermic and positive values as endothermic processes. Transition states along the reaction pathway were determined by using the climbing image nudged elastic band (CI-NEB) method.[56] Transition states were confirmed through frequency analysis, verifying that the transition complex had only one imaginary frequency vibrational mode.

RESULTS AND DISCUSSION

The optimized structure of UiO-66-P-BF_2 is shown in Figure 2a. The structures of UiO-66-P-BF_2 with dissociated H_2 (2H*) and chemically bound CO_2 (denoted CO_2*) are shown in Figure 2b and c, respectively. Key atoms in these structures are labeled to facilitate further discussion. The relaxed lattice parameters for the three structures are given in Table S4 of the Supporting Information and are very close to those of the parent UiO-66; the largest absolute deviation in the lattice parameters is 0.026 Å, and the average absolute deviation is 0.01 Å. We infer from these small changes in the lattice parameters that the functionalized MOFs are most probably stable because it is known experimentally that many functionalized UiO-66 derivatives show quite similar chemical and thermal stabilities with the parent UiO-66.[30] We calculated the pore volume of UiO-P-BF_2 using PLATON.[57] We have also computed the pore volume of UiO-66 and selected functionalized UiO-66 materials that have been synthesized and reported in the literature. We compare the computed pore volumes and porosities of these materials in Table 1. Our

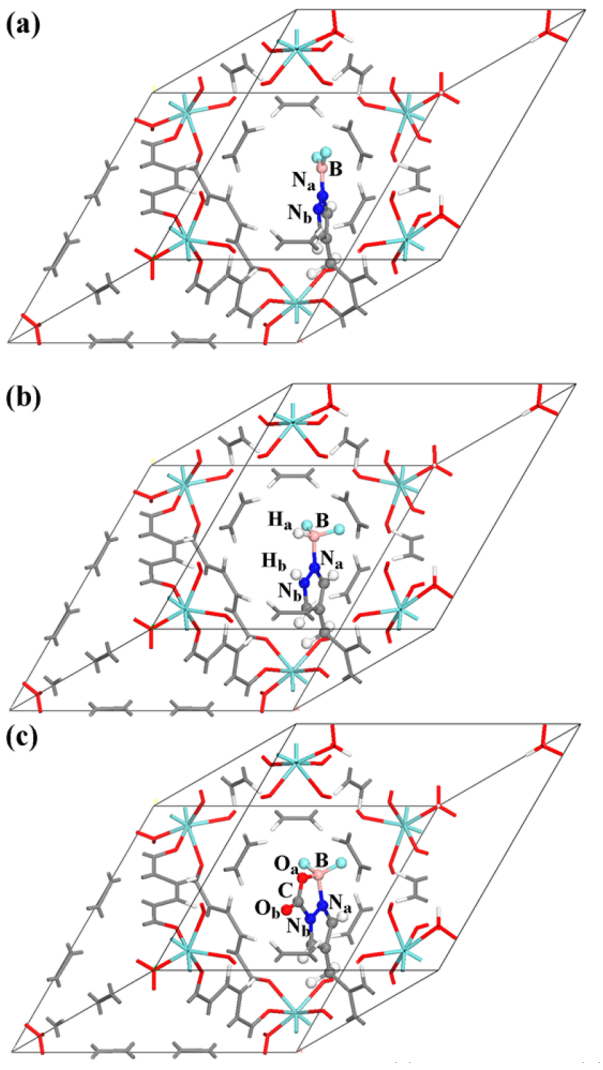

Figure 2. Optimized configurations of (a) UiO-66-P-BF_2, (b) H_2 dissociatively adsorbed in UiO-66-P-BF_2, and (c) CO_2 chemisorbed in UiO-66-P-BF_2.

Table 1. Summary of Pore Volumes and Porosities for Selected Functionalized UiO-66 Materials Calculated from PLATON.[57]

material	pore volume (Å^3)	porosity (%)
UiO-66	1208.2	52.8
UiO-66-P-BF_2	1039.5	45.5
UiO-66-NH-$(CH_2)_3SO_3H$[39]	1023.3	44.7
UiO-66-AM7[28]	978.7	42.8
UiO-66-[FeFe](dcbdt)$(CO)_6$[38]	907.7	39.7

calculated porosity of UiO-66 is in excellent agreement with the reported value of 52.6%.[31] The calculated pore volume of UiO-66-BF_2 is reduced by 169 Å^3 (14%), and the porosity is reduced by 7.3% compared with unfunctionalized UiO-66. The computed pore volumes of UiO-66-NH-$(CH_2)_3SO_3H$,[39] UiO-66-AM7,[28] and UiO-66-[FeFe](dcbdt)$(CO)_6$[38] are also given in Table 1. We have chosen these materials for comparison because they are examples of experimentally realized materials having large functional groups, high porosity, and good thermal and chemical stability. The first two materials were produced by PSM, and the last, by PSE. We note that the pore volume and porosity of UiO-66-P-BF_2 are larger than for the reported functionalized materials listed in Table 1. This comparison is an indication that it is reasonable to expect that UiO-66-P-BF_2 can be synthesized by either PSM or PSE and that it will have both good porosity and stability.

Experiments indicate that the isosteric heat for H_2 adsorption (which is directly related to the absolute value of the adsorption energy) in UiO-66 ranges from about 0.06 to 0.12 eV.[58−60] Experimental and calculated isosteric heats for CO_2 in UiO-66 are ∼0.25[29,36,40,53,60] and 0.27 eV,[34,36] respectively. We have computed physisorption energies of both H_2 and CO_2 in UiO-66 by performing DFT molecular dynamics for exploring the low-energy configurations and optimizing these configurations to local minima (see the Supporting Information and Table S5). The physisorption energies range from −0.06 to −0.17 eV for H_2 and from −0.11 to −0.23 eV for CO_2 in UiO-66, indicating that our dispersion-corrected DFT approach gives reasonably accurate adsorption energies.

Our calculations show that H_2 is heterolytically dissociated in UiO-66-P-BF_2, with one atom (H_a) bound to B and another (H_b) bound to N_b (Figure 2b), generating hydridic (H_a) and protic (H_b) hydrogens. The H_a−B and H_b−N_b bond lengths are 1.219 and 1.018 Å, respectively. The dissociative adsorption energy of H_2 in UiO-66-P-BF_2 is −0.27 eV, which is much less favorable than that for **FLP1** (−0.92 eV; see Table S3 in the Supporting Information). The H_2 dissociation energy profile is shown in Figure 3. We found an intermediate van der Waals (vdW) complex, H_2(vdW), E_{ad} = −0.01 eV, relative to that in

DOI: 10.1021/acscatal.5b00396
ACS Catal. 2015, 5, 2921−2928

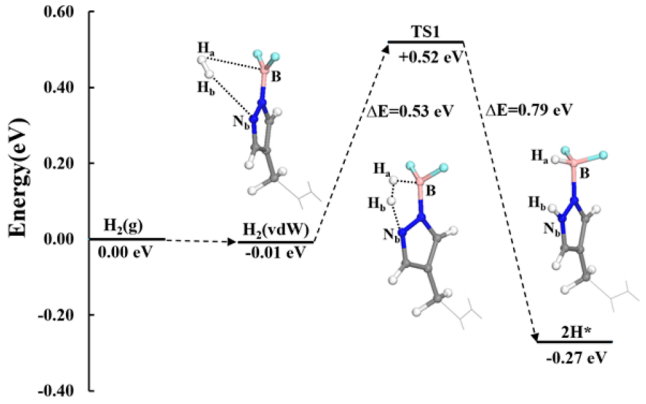

Figure 3. Relative energy profile for dissociation of H_2 in UiO-66-P-BF_2.

the gas phase. Note that this is not the global minimum for H_2 adsorbed in the pore, but is a local minimum on the reaction pathway. The H_a−B and H_b−N_b distances in this physisorbed complex are 3.057 and 2.800 Å, respectively. The transition state for dissociation, TS1, has a barrier of ΔE = 0.53 eV. The barrier for the reverse reaction (recombination) is 0.79 eV.

The reaction pathway for CO_2 chemisorption in UiO-66-P-BF_2 is shown in Figure 4. As with H_2, an intermediate vdW

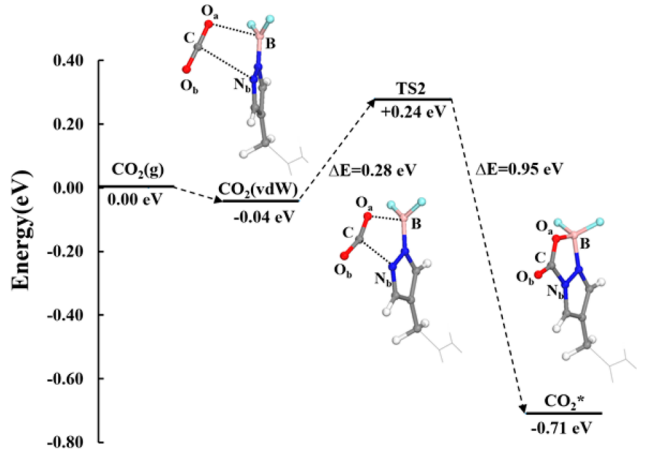

Figure 4. Relative energy profile for CO_2 chemisorption in UiO-66-P-BF_2 from the gas phase.

complex (CO_2(vdW), E_{ad} = −0.04 eV) in the pore was also detected. The O_a−B and C−N_b distances of 3.323 and 3.129 Å in this complex decrease as the reaction proceeds. The transition state (TS2) is shown as an inset in Figure 4. The activation barrier for CO_2 chemisorption is 0.28 eV, and the release of CO_2 from CO_2* requires an activation energy of ∼0.95 eV. The C atom in CO_2* binds to the atom denoted N_b with a bond length of 1.466 Å, and the O atom in CO_2* binds to the B atom with a bond length of 1.526 Å. The C−O_a and C−O_b bonds are elongated to 1.313 and 1.209 Å, respectively, from the gas phase value of 1.176 Å. The O_a−C−O_b angle is reduced to 130.3°, compared with 180° in the gas phase and is indicative of charge transfer to CO_2*. The geometry of CO_2* in UiO-66-P-BF_2 is very close to that of CO_2 bound to **FLP1**.[55] The adsorption energy of CO_2 in UiO-66-P-BF_2 is −0.71 eV relative to that in the gas phase, which is slightly less favorable than that for **FLP1** (−0.87 eV; see Table S3 in the Supporting Information).

Our calculations demonstrate that the LP in UiO-66-P-BF_2 retains the chemical activity of **FLP1** toward H_2 and CO_2. We now consider reaction pathways for H_2 reacting with CO_2 in UiO-66-P-BF_2.

We have identified two reaction pathways for CO_2 hydrogenation within UiO-66-P-BF_2, as shown in Figure 5. One pathway involves physisorbed CO_2 reacting with chemisorbed 2H* (green line in Figure 5), and the other involves physisorbed H_2 reacting with CO_2* (red line in Figure 5). The first part of the green line in Figure 5 is the same as in Figure 3 for dissociation of H_2. The adsorption energy of CO_2 adsorbing in the pore with 2H* is −0.21 eV relative to CO_2 in the gas phase. The transition state for CO_2 hydrogenation (TS3 in Figure 5) has a barrier of 0.47 eV. We note that the addition of the hydridic and protic hydrogens occurs in a concerted fashion, rather than a stepwise mechanism. The concerted mechanism for CO_2 reduction has been predicted to be a lower energy pathway than the stepwise mechanism.[61] The formic acid product has an energy that is 0.21 eV lower than the gas phase H_2 and CO_2 reactants. Desorption of HCOOH to the gas phase requires 0.34 eV of energy, raising the final product state 0.13 eV above the reactants, which is consistent with hydrogenation of CO_2 being endothermic.

The second reaction pathway (red line in Figure 5) starts with chemisorption of CO_2 from the gas phase onto UiO-66-P-BF_2, followed by the adsorption of H_2 to form a coadsorbed complex (H_2 + CO_2*). The reaction barrier for hydrogenation of the activated CO_2* is 2.65 eV (TS4 in Figure 5). This barrier is similar to the gas phase uncatalyzed reaction barrier (Figure 6), but leads to the formation of chemisorbed HCO and OH ([HCO+OH]*) instead of HCOOH. This illustrates that P-BF_2 binds CO_2 too strongly to produce a low barrier pathway to hydrogenation of CO_2, in accordance with the general Sabatier principle. Moreover, this pathway leads to the wrong product.

Our calculations show that the desired CO_2 reduction mechanism proceeds via H_2 heterolytic dissociation, followed by CO_2 reaction with the chemisorbed H atoms to produce HCOOH. Given that CO_2 is much more strongly bound to the LP than H_2, practical use of UiO-66-P-BF_2 for CO_2 reduction will require that this material be exposed first to H_2 and then to CO_2 in sequence to prevent poisoning of the LP by CO_2. It is also important to prevent H_2O exposure to the LP sites because of its tendency to strongly bind to similar moieties.[62] This could be accomplished by embedding the LP sites in the core of a core−shell MOF capable of admitting CO_2 and H_2 while rejecting H_2O, such as that designed by Li et al.[63] The requirement of sequential exposure of UiO-66-P-BF_2 to H_2 followed by CO_2 would prohibit its practical use. Nevertheless, our calculations provide a proof-of-concept that functional groups can be devised from computations that dramatically reduce the barriers for CO_2 reduction. Moreover, the large variety of MOFs and functional groups available means that it may be possible to design a material without the need for sequential adsorption by utilizing functional groups specifically targeted to binding H_2 and CO_2 separately.

We computed reaction pathways for hydrogenation of CO_2 in the gas phase (not in UiO-66) via three mechanisms: (i) uncatalyzed, (ii) catalyzed by **FLP1**, and (iii) catalyzed by P-BF_2. These calculations shed light on the role of UiO-66 and P-BF_2 in UiO-66-P-BF_2. The results of these calculations are shown in Figure 6, and the structural details are included in Figure S7 of the Supporting Information. The reaction pathway

DOI: 10.1021/acscatal.5b00396
ACS Catal. 2015, 5, 2921−2928

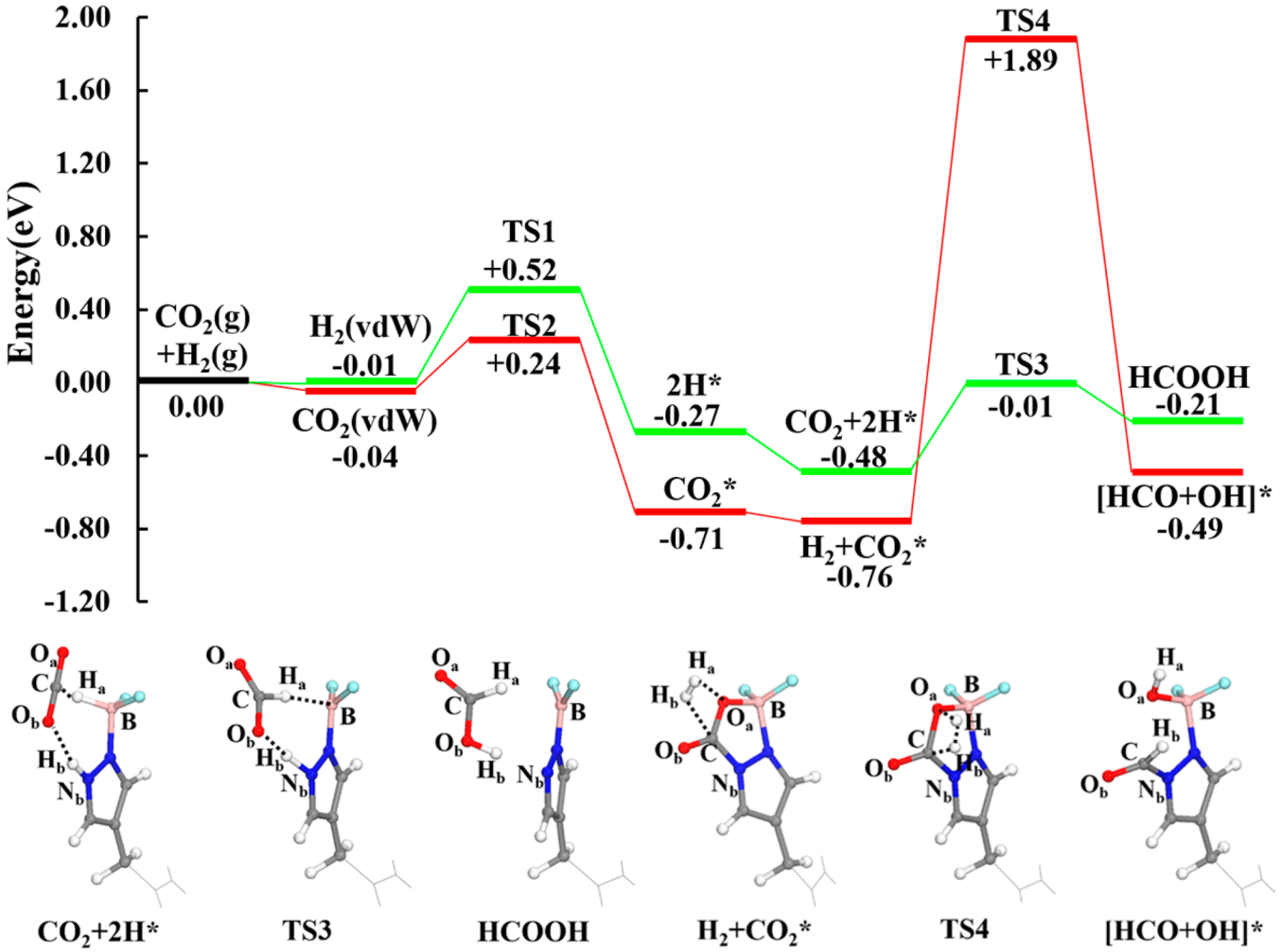

Figure 5. Relative potential energy surfaces for two different CO_2 hydrogenation pathways in UiO-66-P-BF_2. The energy reference is CO_2(g) + H_2(g) and the empty UiO-66-P-BF_2. Selected configurations from the potential energy surfaces are given below the graph.

for hydrogenation of CO_2 in the gas phase has a barrier of 2.76 (2.70) eV with (without) ZPE corrections. This compares reasonably well with experimental results 2.85 eV[64] and is somewhat lower than the value of 3.17 eV computed from the M06-L functional[65,66] without ZPE corrections reported by Maihom et al.[67]

The reaction pathway for hydrogenation of CO_2 catalyzed by **FLP1** is very similar to the pathway we computed for UiO-66-P-BF_2. The two barriers are 0.45 and 0.91 eV for H_2 dissociation and HCOOH formation, respectively, as can be seen from the orange line in Figure 6. The H_2 dissociation barrier in **FLP1** is slightly lower than in UiO-66-P-BF_2, but the CO_2 hydrogenation barrier is considerably larger (0.47 eV in UiO-66-P-BF_2 versus 0.91 eV in **FLP1**), indicating that the reaction rate in UiO-66-P-BF_2 will be larger than for **FLP1**. The gas phase P-BF_2 reaction is shown as the blue line in Figure 6. The reaction barrier for H_2 dissociation is 0.73 and 0.53 eV for CO_2 hydrogenation. The CO_2 hydrogenation barrier is close to that in UiO-66-P-BF_2; in contrast, the H_2 dissociation barrier is 0.2 eV higher. Comparison of these systems gives the following observations: (1) the dissociation barrier for H_2 follows the order P-BF_2 > UiO-66-P-BF_2 > **FLP1**; (2) the CO_2 hydrogenation barrier follows the order **FLP1** > P-BF_2 > UiO-66-P-BF_2; (3) the apparent effects of the UiO-66 framework on the reactivity of P-BF_2 are to (i) reduce the barrier for H_2 dissociation, (ii) increase the adsorption energy for 2H*, and (iii) reduce the barrier for CO_2 hydrogenation.

An explanation for the trends in H_2 dissociation barriers can be found by examining the torsion angles defined by the two nitrogens on the pyrazole ring and the boron and the carbon (**FLP1**) or fluorine (P-BF_2 and UiO-66-P-BF_2) atoms in these three systems (see Table S6 and Figure S16 in the Supporting Information). The torsion angle in **FLP1** is the largest at 44.89°, followed by UiO-66-P-BF_2 with 22.84°, whereas P-BF_2 has the smallest angle of 0.08° (see Table S6 in the Supporting Information). The larger torsion angle facilitates H_2 dissociation, as can be seen from the torsion angles resulting after chemisorption of H_2 (2H*; Table S6 in the Supporting Information). The calculated torsional rotation energy for the BF_2 group in P-BF_2 going from 0° to 22.84° (44.89°) is 0.10 (0.31) eV; hence, the decrease in the H_2 dissociation barrier going from P-BF_2 to UiO-66-P-BF_2 is due to the confinement of P-BF_2 in UiO-66, which gives rise to the observed equilibrium torsion angle of 22.84°. Moreover, the steric hindrance of the bulky C_6F_5 groups in **FLP1** give rise to the large torsion angle that lowers the barrier for H_2 dissociation. Hence, in this case, steric hindrance enhances H_2's interacting with the Lewis pairs,[68−70] rather than increasing the reaction barrier.[18]

DOI: 10.1021/acscatal.5b00396
ACS Catal. 2015, 5, 2921−2928

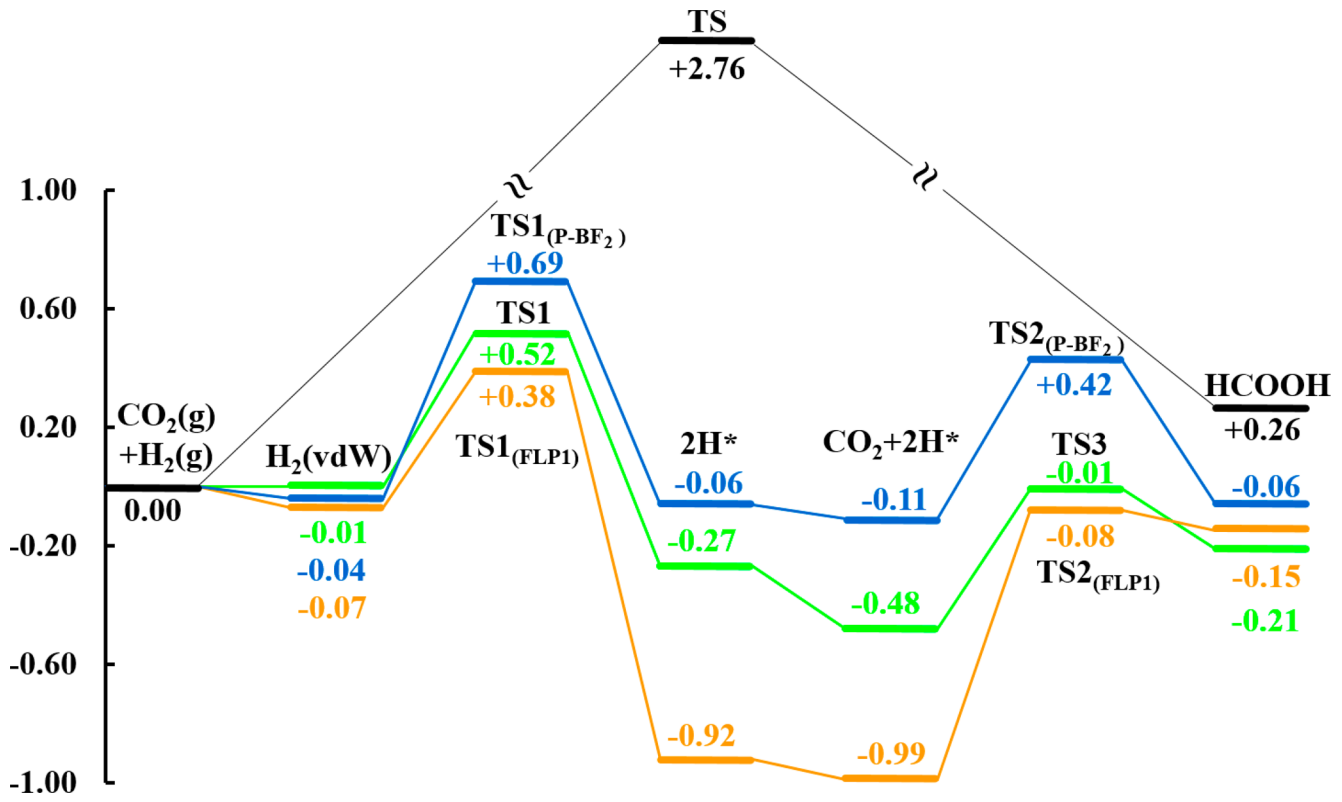

Figure 6. Relative potential energy surfaces for gas phase CO_2 hydrogenation without a catalyst (black), catalyzed by **FLP1** (orange), and catalyzed by P-BF_2 (blue). The UiO-66-P-BF_2 pathway from Figure 5 is shown for comparison (green).

The difference in the CO_2 hydrogenation barriers between **FLP1** and P-BF_2 or UiO-66-P-BF_2 is attributed to the much stronger binding energy for H_2 according on **FLP1**, in accordance with the Brønsted−Evans−Polanyi (BEP) principle.[71−73] The stronger binding energy of H_2 in **FLP1** is consistent with the shorter distance between the Lewis acid (B) and base (N_b) sites and stronger acidity and basicity in **FLP1** than in P-BF_2 (see Table S6−S7 in the Supporting Information).[74] The difference between the hydrogenation barriers for P-BF_2 and UiO-66-P-BF_2 is fairly small (0.04 eV), although the difference in the H_2 chemisorption energies is 0.21 eV, in apparent disagreement with the BEP principle. We have verified that the difference in the H_2 adsorption energies is not due to differences in charge distribution or vdW interactions (see Tables S8 and S9 in the Supporting Information). In contrast, there is significant vdW stabilization (0.33 eV) of CO_2 in UiO-66-P-BF_2 compared with P-BF_2, as can be seen by comparing the adsorption energies of CO_2 on UiO-66-P-BF_2/2H* with and without vdW interactions (Table S9 in the Supporting Information). It is surprising that the hydrogenation barriers are similar on P-BF_2/2H* and UiO-66-P-BF_2/2H*, given that the H_2 adsorption energies are significantly different. The reason for this is likely due to differences in the initial geometries of the CO_2 vdW complexes, denoted CO_2 + 2H* and shown in Figure 5 and Figure S7c of the Supporting Information for UiO-66-P-BF_2/CO_2+2H* and P-BF_2/CO_2+2H*, respectively. The two O_b−H_b bond lengths (Supporting Information) are 1.999 and 2.269 Å, respectively. The shorter O_b−H_b bond length in UiO-66-P-BF_2/CO_2 + 2H* is due to confinement effects, perhaps partially as a result of vdW forces. This is an example of how the geometry of the pore might modulate a reaction barrier in ways not easily foreseen.

SUMMARY AND OUTLOOK

We have demonstrated that functionalization of UiO-66 with a Lewis pair moiety results in an apparently stable structure with only very minor perturbation to the lattice parameters. There are many routes for synthesizing MOFs having functional groups of size and complexity similar to that of UiO-66-P-BF_2; a hypothetical pathway for the synthesis of UiO-66-P-BF_2 based on combining ideas based on synthesis of **FLP1** and mixed ligand synthesis is given in the Supporting Information. The Lewis pair retains its chemical activity when bound in the pore, being able to facilely bind H_2 and CO_2. Furthermore, CO_2 can be reduced via a low energy barrier pathway by first exposing UiO-66-P-BF_2 to H_2, giving heterolytic dissociation, followed by exposure to CO_2. The dissociation of H_2 has a slightly higher barrier than hydrogenation of CO_2, which occurs in a single step. The reaction barriers are much lower than those reported in the literature for heterogeneous reduction of CO_2 to HCOOH, which are typically on the order of 1 eV.[10−15] Importantly, the barriers are comparable with or lower than the lowest barriers reported for homogeneous reduction of CO_2 with heterogeneous organometallic catalysts.[75−77] Thus, our catalyst combines the advantages of homogeneous catalysts (ease of catalyst recovery, high mass transfer, etc.) with the advantages of homogeneous catalysts (low reaction barriers).[22,23] Moreover, the catalytic sites are metal-free Lewis acid and base pairs (the framework contains metals, but these are not part of the catalytic functional groups in the pores).

Our calculations indicate that the critical step in the reaction is splitting H_2 into hydridic and protic species to facilitate

DOI: 10.1021/acscatal.5b00396
ACS Catal. 2015, 5, 2921−2928

concerted addition of hydrogens to form HCOOH. This happens without activating the CO_2. Conversely, starting from an activated CO_2* complex without activating the H_2 leads to a very high barrier for hydrogenation and produces chemisorbed formyl and hydroxyl moieties rather than the desired HCOOH product. This is due to CO_2's being bound too strongly to UiO-66-P-BF_2. Hence, for the UiO-66-P-BF_2 catalyst to work in practice, one would have to expose the material first to H_2 and then to CO_2 to avoid the competing reaction and potential poisoning of the catalyst. This requirement is a major drawback for UiO-66-P-BF_2 that would preclude its practical use. An ideal catalyst would selectively bind CO_2 more weakly than the P-BF_2 moiety while providing a binding site that selectively dissociates H_2 similar to P-BF_2. This would require a MOF having two complementary binding sites with the pore positioned such that the 2H* and CO_2* have the correct binding energy (Sabatier principle) and mutual orientation (3-dimentional structure) to minimize the overall reaction barriers. This kind of control over binding sites and orientations is very difficult to achieve in typical metal or metal oxide catalysts but may be possible in tailored functionalized MOFs. We will investigate the activity of other Lewis pair functional groups and addition of multiple binding sites per pore for simultaneous activation of CO_2 and H_2 in future work.

■ ASSOCIATED CONTENT

Supporting Information

The following file is available free of charge on the ACS Publications website at DOI: 10.1021/acscatal.5b00396.

Computational methods, accuracy tests, optimized lattice constants, structural details, reaction energy profiles, proposed synthetic pathway (PDF)

■ AUTHOR INFORMATION

Corresponding Author

*E-mail: karlj@pitt.edu.

Notes

The authors declare no competing financial interests.

■ ACKNOWLEDGMENTS

We gratefully acknowledge the support from the U.S. Department of Energy (Grant No. DE-FG02-10ER16165). We thank N. L. Rosi, E. J. Beckman, and J. A. Keith for many helpful discussions. The computations were performed at the University of Pittsburgh's Center for Simulation & Modeling and at the Extreme Science and Engineering Discovery Environment (XSEDE) under project TG-CHE140046.

■ REFERENCES

(1) Aresta, M.; Dibenedetto, A. *Dalton Trans.* **2007**, 2975−2992.
(2) Olah, G. A.; Prakash, G. K. S.; Goeppert, A. *J. Am. Chem. Soc.* **2011**, *133*, 12881−12898.
(3) Ma, J.; Sun, N.; Zhang, X.; Zhao, N.; Xiao, F.; Wei, W.; Sun, Y. *Catal. Today* **2009**, *148*, 221−231.
(4) Qiao, J.; Liu, Y.; Hong, F.; Zhang, J. *Chem. Soc. Rev.* **2014**, *43*, 631−675.
(5) Studt, F.; Sharafutdinov, I.; Abild-Pedersen, F.; Elkjær, C. F.; Hummelshøj, J. S.; Dahl, S.; Chorkendorff, I.; Nørskov, J. K. *Nat. Chem.* **2014**, *6*, 320−324.
(6) Wang, W.; Wang, S.; Ma, X.; Gong, J. *Chem. Soc. Rev.* **2011**, *40*, 3703−3727.
(7) Liu, Q.; Wu, L.; Jackstell, R.; Beller, M. *Nat. Commun.* **2015**, *6*, 5933.
(8) Federsel, C.; Jackstell, R.; Beller, M. *Angew. Chem., Int. Ed.* **2010**, *49*, 6254−6257.
(9) Cheng, D.; Negreiros, F. R.; Aprà, E.; Fortunelli, A. *ChemSusChem* **2013**, *6*, 944−965.
(10) Peng, G.; Sibener, S. J.; Schatz, G. C.; Mavrikakis, M. *Surf. Sci.* **2012**, *606*, 1050−1055.
(11) Peng, G.; Sibener, S. J.; Schatz, G. C.; Ceyer, S. T.; Mavrikakis, M. *J. Phys. Chem. C* **2011**, *116*, 3001−3006.
(12) Vesselli, E.; Rizzi, M.; De Rogatis, L.; Ding, X.; Baraldi, A.; Comelli, G.; Savio, L.; Vattuone, L.; Rocca, M.; Fornasiero, P.; Baldereschi, A.; Peressi, M. *J. Phys. Chem. Lett.* **2009**, *1*, 402−406.
(13) Pan, Y.-x.; Liu, C.-j.; Ge, Q. *J. Catal.* **2010**, *272*, 227−234.
(14) Grabow, L. C.; Mavrikakis, M. *ACS Catal.* **2011**, *1*, 365−384.
(15) Zhao, Y.-F.; Yang, Y.; Mims, C.; Peden, C. H. F.; Li, J.; Mei, D. *J. Catal.* **2011**, *281*, 199−211.
(16) Ashley, A. E.; O'Hare, D. *Curr. Top. Chem.* **2013**, *334*, 191−217.
(17) Stephan, D. W.; Erker, G. *Angew. Chem., Int. Ed.* **2010**, *49*, 46−76.
(18) Courtemanche, M.-A.; Légaré, M.-A.; Maron, L.; Fontaine, F.-G. *J. Am. Chem. Soc.* **2014**, *136*, 10708−10717.
(19) Lim, C.-H.; Holder, A. M.; Hynes, J. T.; Musgrave, C. B. *Inorg. Chem.* **2013**, *52*, 10062−10066.
(20) Ménard, G.; Stephan, D. W. *J. Am. Chem. Soc.* **2010**, *132*, 1796−1797.
(21) Sgro, M. J.; Domer, J.; Stephan, D. W. *Chem. Commun.* **2012**, *48*, 7253−7255.
(22) Zhang, X.; Llabrés i Xamena, F. X.; Corma, A. *J. Catal.* **2009**, *265*, 155−160.
(23) Notestein, J. M.; Katz, A. *Chem. - Eur. J.* **2006**, *12*, 3954−3965.
(24) Bae, Y.-S.; Snurr, R. Q. *Angew. Chem., Int. Ed.* **2011**, *50*, 11586−11596.
(25) Han, S.; Huang, Y.; Watanabe, T.; Dai, Y.; Walton, K. S.; Nair, S.; Sholl, D. S.; Meredith, J. C. *ACS Comb. Sci.* **2012**, *14*, 263−267.
(26) Wilmer, C. E.; Farha, O. K.; Bae, Y.-S.; Hupp, J. T.; Snurr, R. Q. *Energy Environ. Sci.* **2012**, *5*, 9849−9856.
(27) Cavka, J. H.; Jakobsen, S.; Olsbye, U.; Guillou, N.; Lamberti, C.; Bordiga, S.; Lillerud, K. P. *J. Am. Chem. Soc.* **2008**, *130*, 13850−13851.
(28) Garibay, S. J.; Cohen, S. M. *Chem. Commun.* **2010**, *46*, 7700−7702.
(29) Huang, Y.; Qin, W.; Li, Z.; Li, Y. *Dalton Trans.* **2012**, *41*, 9283−9285.
(30) Kim, M.; Cohen, S. M. *CrystEngComm* **2012**, *14*, 4096−4104.
(31) Wu, H.; Yildirim, T.; Zhou, W. *J. Phys. Chem. Lett.* **2013**, *4*, 925−930.
(32) Valenzano, L.; Civalleri, B.; Chavan, S.; Bordiga, S.; Nilsen, M. H.; Jakobsen, S.; Lillerud, K. P.; Lamberti, C. *Chem. Mater.* **2011**, *23*, 1700−1718.
(33) Biswas, S.; Zhang, J.; Li, Z. B.; Liu, Y. Y.; Grzywa, M.; Sun, L. X.; Volkmer, D.; Van der Voort, P. *Dalton Trans.* **2013**, *42*, 4730−4737.
(34) Yang, Q.; Wiersum, A. D.; Llewellyn, P. L.; Guillerm, V.; Serre, C.; Maurin, G. *Chem. Commun.* **2011**, *47*, 9603−9605.
(35) Yang, Q. Y.; Guillerm, V.; Ragon, F.; Wiersum, A. D.; Llewellyn, P. L.; Zhong, C. L.; Devic, T.; Serre, C.; Maurin, G. *Chem. Commun.* **2012**, *48*, 9831−9833.
(36) Yang, Q.; Wiersum, A. D.; Jobic, H.; Guillerm, V.; Serre, C.; Llewellyn, P. L.; Maurin, G. *J. Phys. Chem. C* **2011**, *115*, 13768−13774.
(37) Yang, Q. Y.; Wiersum, A. D.; Llewellyn, P. L.; Guillerm, V.; Serred, C.; Maurin, G. *Chem. Commun.* **2011**, *47*, 9603−9605.
(38) Pullen, S.; Fei, H.; Orthaber, A.; Cohen, S. M.; Ott, S. *J. Am. Chem. Soc.* **2013**, *135*, 16997−17003.
(39) Luan, Y.; Zheng, N. N.; Qi, Y.; Yu, J.; Wang, G. *Eur. J. Inorg. Chem.* **2014**, 4268−4272.
(40) Cmarik, G. E.; Kim, M.; Cohen, S. M.; Walton, K. S. *Langmuir* **2012**, *28*, 15606−15613.
(41) Vermoortele, F.; Bueken, B.; Le Bars, G.; Van de Voorde, B.; Vandichel, M.; Houthoofd, K.; Vimont, A.; Daturi, M.; Waroquier, M.; Van Speybroeck, V.; Kirschhock, C.; De Vos, D. E. *J. Am. Chem. Soc.* **2013**, *135*, 11465−11468.

DOI: 10.1021/acscatal.5b00396
ACS Catal. 2015, 5, 2921−2928

(42) VandeVondele, J.; Krack, M.; Mohamed, F.; Parrinello, M.; Chassaing, T.; Hutter, J. *Comput. Phys. Commun.* **2005**, *167*, 103−128.
(43) Grimme, S.; Antony, J.; Ehrlich, S.; Krieg, H. *J. Chem. Phys.* **2010**, *132*, 154104.
(44) Wang, C.; deKrafft, K. E.; Lin, W. *J. Am. Chem. Soc.* **2012**, *134*, 7211−7214.
(45) Wang, C.; Xie, Z.; deKrafft, K. E.; Lin, W. *J. Am. Chem. Soc.* **2011**, *133*, 13445−13454.
(46) Kim, M.; Cahill, J. F.; Su, Y.; Prather, K. A.; Cohen, S. M. *Chem. Sci.* **2012**, *3*, 126−130.
(47) Cohen, S. M. *Chem. Rev.* **2012**, *112*, 970−1000.
(48) Kim, M.; Garibay, S. J.; Cohen, S. M. *Inorg. Chem.* **2011**, *50*, 729−731.
(49) Wang, Z.; Cohen, S. M. *Chem. Soc. Rev.* **2009**, *38*, 1315−1329.
(50) Perdew, J. P.; Burke, K.; Ernzerhof, M. *Phys. Rev. Lett.* **1996**, *77*, 3865−3868.
(51) Goedecker, S.; Teter, M.; Hutter, J. *Phys. Rev. B: Condens. Matter Mater. Phys.* **1996**, *54*, 1703−1710.
(52) Frisch, M. J.; Trucks, G. W.; Schlegel, H. B.; Scuseria, G. E.; Robb, M. A.; Cheeseman, J. R.; Scalmani, G.; Barone, V.; Mennucci, B.; Petersson, G. A.; Nakatsuji, H.; Caricato, M.; Li, X.; Hratchian, H. P.; Izmaylov, A. F.; Bloino, J.; Zheng, G.; Sonnenberg, J. L.; Hada, M.; Ehara, M.; Toyota, K.; Fukuda, R.; Hasegawa, J.; Ishida, M.; Nakajima, T.; Honda, Y.; Kitao, O.; Nakai, H.; Vreven, T.; Montgomery Jr., J. A.; Peralta, J. E.; Ogliaro, F.; Bearpark, M. J.; Heyd, J.; Brothers, E. N.; Kudin, K. N.; Staroverov, V. N.; Kobayashi, R.; Normand, J.; Raghavachari, K.; Rendell, A. P.; Burant, J. C.; Iyengar, S. S.; Tomasi, J.; Cossi, M.; Rega, N.; Millam, N. J.; Klene, M.; Knox, J. E.; Cross, J. B.; Bakken, V.; Adamo, C.; Jaramillo, J.; Gomperts, R.; Stratmann, R. E.; Yazyev, O.; Austin, A. J.; Cammi, R.; Pomelli, C.; Ochterski, J. W.; Martin, R. L.; Morokuma, K.; Zakrzewski, V. G.; Voth, G. A.; Salvador, P.; Dannenberg, J. J.; Dapprich, S.; Daniels, A. D.; Farkas, Ö.; Foresman, J. B.; Ortiz, J. V.; Cioslowski, J.; Fox, D. J. *Gaussian 09 Revision B.01*, 2009.
(53) Wiersum, A. D.; Soubeyrand-Lenoir, E.; Yang, Q.; Moulin, B.; Guillerm, V.; Yahia, M. B.; Bourrelly, S.; Vimont, A.; Miller, S.; Vagner, C.; Daturi, M.; Clet, G.; Serre, C.; Maurin, G.; Llewellyn, P. L. *Chem. - Asian J.* **2011**, *6*, 3270−3280.
(54) Theuergarten, E.; Schluns, D.; Grunenberg, J.; Daniliuc, C. G.; Jones, P. G.; Tamm, M. *Chem. Commun.* **2010**, *46*, 8561−8563.
(55) Theuergarten, E.; Schlosser, J.; Schluns, D.; Freytag, M.; Daniliuc, C. G.; Jones, P. G.; Tamm, M. *Dalton Trans.* **2012**, *41*, 9101−9110.
(56) Henkelman, G.; Uberuaga, B. P.; Jónsson, H. *J. Chem. Phys.* **2000**, *113*, 9901−9904.
(57) Spek, A. *J. Appl. Crystallogr.* **2003**, *36*, 7−13.
(58) Ren, J.; Segakweng, T.; Langmi, H.; Musyoka, N.; North, B.; Mathe, M.; Bessarabov, D. *Int. J. Mater. Res.* **2014**, *105*, 516−519.
(59) Zlotea, C.; Phanon, D.; Mazaj, M.; Heurtaux, D.; Guillerm, V.; Serre, C.; Horcajada, P.; Devic, T.; Magnier, E.; Cuevas, F.; Ferey, G.; Llewellyn, P. L.; Latroche, M. *Dalton Trans.* **2011**, *40*, 4879−4881.
(60) Abid, H. R.; Tian, H.; Ang, H.-M.; Tade, M. O.; Buckley, C. E.; Wang, S. *Chem. Eng. J.* **2012**, *187*, 415−420.
(61) Zimmerman, P. M.; Zhang, Z.; Musgrave, C. B. *Inorg. Chem.* **2010**, *49*, 8724−8728.
(62) Stephan, D. W.; Greenberg, S.; Graham, T. W.; Chase, P.; Hastie, J. J.; Geier, S. J.; Farrell, J. M.; Brown, C. C.; Heiden, Z. M.; Welch, G. C.; Ullrich, M. *Inorg. Chem.* **2011**, *50*, 12338−12348.
(63) Li, T.; Sullivan, J. E.; Rosi, N. L. *J. Am. Chem. Soc.* **2013**, *135*, 9984−9987.
(64) Saito, K.; Kakumoto, T.; Kuroda, H.; Torii, S.; Imamura, A. *J. Chem. Phys.* **1984**, *80*, 4989−4996.
(65) Zhao, Y.; Truhlar, D. G. *Acc. Chem. Res.* **2008**, *41*, 157−167.
(66) Zhao, Y.; Truhlar, D. G. *J. Phys. Chem. C* **2008**, *112*, 6860−6868.
(67) Maihom, T.; Wannakao, S.; Boekfa, B.; Limtrakul, J. *J. Phys. Chem. C* **2013**, *117*, 17650−17658.
(68) Camaioni, D. M.; Ginovska-Pangovska, B.; Schenter, G. K.; Kathmann, S. M.; Autrey, T. *J. Phys. Chem. A* **2012**, *116*, 7228−7237.
(69) Wang, Z.; Lu, G.; Li, H.; Zhao, L. *Chin. Sci. Bull.* **2010**, *55*, 239−245.
(70) Rokob, T. A.; Hamza, A.; Stirling, A.; Soós, T.; Pápai, I. *Angew. Chem., Int. Ed.* **2008**, *47*, 2435−2438.
(71) Bligaard, T.; Nørskov, J. K.; Dahl, S.; Matthiesen, J.; Christensen, C. H.; Sehested, J. *J. Catal.* **2004**, *224*, 206−217.
(72) Michaelides, A.; Liu, Z. P.; Zhang, C. J.; Alavi, A.; King, D. A.; Hu, P. *J. Am. Chem. Soc.* **2003**, *125*, 3704−3705.
(73) Jiang, T.; Mowbray, D. J.; Dobrin, S.; Falsig, H.; Hvolbæk, B.; Bligaard, T.; Nørskov, J. K. *J. Phys. Chem. C* **2009**, *113*, 10548−10553.
(74) Rokob, T. A.; Hamza, A.; Pápai, I. *J. Am. Chem. Soc.* **2009**, *131*, 10701−10710.
(75) Hou, C.; Jiang, J.; Zhang, S.; Wang, G.; Zhang, Z.; Ke, Z.; Zhao, C. *ACS Catal.* **2014**, *4*, 2990−2997.
(76) Ahlquist, M. S. G. *J. Mol. Catal. A: Chem.* **2010**, *324*, 3−8.
(77) Urakawa, A.; Jutz, F.; Laurenczy, G.; Baiker, A. *Chem. - Eur. J.* **2007**, *13*, 3886−3899.

DOI: 10.1021/acscatal.5b00396
ACS Catal. 2015, 5, 2921−2928